International Journal of Minerals, Metallurgy and Materials
Volume 26, Number 7, July 2019, Page 822
https://doi.org/10.1007/s12613-019-1795-8

Thermodynamic studies on gas-based reduction of vanadium titano-magnetite pellets

Jun-wei Chen, Yang Jiao, and Xi-dong Wang

Department of Energy and Resources Engineering, College of Engineering, Peking University, Beijing 100871, China
(Received: 12 September 2018; revised: 16 November 2018; accepted: 22 November 2018)

Abstract: Numerous studies have focused on the reduction thermodynamics of ordinary iron ore; by contrast, the literature contains few thermodynamic studies on the gas-based reduction of vanadium titano-magnetite (VTM) in mixed atmospheres of H_2, CO, H_2O, CO_2, and N_2. In this paper, thermodynamic studies on the reduction of oxidized VTM pellets were systematically conducted in an atmosphere of a C–H–O system as a reducing agent. The results indicate that VTM of an equivalent valence state is more difficult to reduce than ordinary iron ore. A reduction equilibrium diagram using the C–H–O system as a reducing agent was obtained; it clearly describes the reduction process. Experiments were performed to investigate the effects of the reduction temperature, the gas composition, and two types of iron ores on the reduction of oxidized VTM pellets. The results show that the final reduction degree increases with increasing reduction temperature, increasing molar ratio of $H_2/(H_2 + CO)$, and decreasing H_2O, CO_2, and N_2 contents. In addition, the reduction processes under various conditions are discussed. All of the results of the reduction experiments are consistent with those of theoretical thermodynamic analysis. This study is expected to provide valuable thermodynamic theory on the industrial applications of VTM.

Keywords: vanadium titano-magnetite; gas-based reduction; C–H–O system; thermodynamics

1. Introduction

Vanadium titano-magnetite (VTM) is a compound mineral that consists of titanium (Ti), iron (Fe), vanadium (V), and various rare metals [1–3]. VTM is attracting increasing attention because of its critical value to advanced technologies [4–5]. Analysis has shown that China possesses approximately 1×10^{10} t VTM. The key to utilizing VTM is separating Fe, V, and Ti efficiently. The technologies that utilize VTM can be classified into two types: blast furnace (BF) processes and non-BF processes [6]. Compared with the non-BF processes, BF technology has reached a more mature state because of its long history of development in China and Russia. However, there are still several problems inherent in the BF process. First, coke resources are very limited, which restricts the development of BF technology. Second, the limestone added as a solvent in BFs hinders the recycling of Ti in VTM because of the reaction between TiO_2 and limestone, which can produce perovskite [7–9]. Many studies have investigated the use of VTM in non-BF processes in addition to the development of some technological processes for the utilization of VTM. A number of scholars have argued that the two most promising prospective processes are the pre-reduction electric furnace smelting process and the reduction roasting magnetic separation process because of their high recovery rates of valuable elements and their low processing costs [10].

Reduction is an essential procedure in both the pre-reduction electric furnace smelting process and the reduction roasting magnetic separation process. Hence, it is extremely important to investigate reduction thermodynamics of VTM. Much research has been published on the reduction thermodynamics of ordinary iron ore [11–17]. However, the crystalline structure of VTM is complicated because the Ti and Fe are symbiotically close to each other [10]. Thus, the reduction thermodynamics of VTM differs from that of ordinary iron ore. Only a few studies have investigated the thermodynamics of VTM during the gas-based reduction process. Furthermore, many of these studies used pure hydrogen or carbon monoxide as a reducing agent, which can cause erroneous results because a mixture of H_2 and CO gases is often used as the reducing

Corresponding author: Xi-dong Wang E-mail: xidong@pku.edu.cn

agent in actual industrial processes. In addition, a large amount of nitrogen, carbon dioxide, and water vapor can exist in the system, which can weaken the reducing ability of the reducing agent. Thus, exploring the thermodynamic behavior of VTM in this complex atmosphere is important.

This work presents thermodynamic studies on the gas-based reduction of oxidized VTM pellets, carried out in a systematic fashion. Specifically, the influences of reduction temperature, gas composition, and the specific type of iron ore used on the reduction thermodynamics were investigated on the basis of theoretical calculations and experimental results.

2. Thermodynamic theory analysis

We focus on the titanium-bearing phases because thermodynamic studies of vanadium-bearing phases have already been reported [18–21]. On the basis of previous research, the reduction reactions in a CO or H_2 atmosphere regarding ordinary iron ore are described by reactions (1)–(8) in Table 1. Similarly, the most likely reactions in oxidized VTM pellets in reducing atmospheres of CO or H_2 are described by reactions (1)–(18) in Table 1, where the corresponding standard Gibbs free energy changes ($\Delta G^{\ominus}$) of all

Table 1. $\Delta G^{\ominus}$ and K of the reduction reactions in oxidized VTM pellets [22–24]

No.	Reaction	$\Delta G^{\ominus}$ / (kJ·mol^{-1})	lg$K$
(1)	$3Fe_2O_3 + CO = 2Fe_3O_4 + CO_2$	$-7100 - 13.42T$	$\frac{1552}{T} + 2.93$
(2)	$3Fe_2O_3 + H_2 = 2Fe_3O_4 + H_2O$	$160 - 19.98T$	$-\frac{35}{T} + 4.37$
(3)	$Fe_3O_4 + CO = 3FeO + CO_2$	$7965 - 9.88T$	$-\frac{1741}{T} + 2.16$
(4)	$Fe_3O_4 + H_2 = 3FeO + H_2O$	$15110 - 16.4T$	$-\frac{3302}{T} + 3.584$
(5)	$\frac{1}{4}Fe_3O_4 + CO = \frac{3}{4}Fe + CO_2$	$-1580 + 1.45T$	$\frac{345.3}{T} - 0.317$
(6)	$\frac{1}{4}Fe_3O_4 + H_2 = \frac{3}{4}Fe + H_2O$	$5560 - 5.08T$	$-\frac{1215}{T} + 1.11$
(7)	$FeO + CO = Fe + CO_2$	$-4702 + 5.15T$	$\frac{1028}{T} - 1.126$
(8)	$FeO + H_2 = Fe + H_2O$	$2389 - 1.34T$	$-\frac{522.1}{T} + 0.293$
(9)	$Fe_2TiO_5 + CO = Fe_2TiO_4 + CO_2$	$-9880 - 4.92T$	$\frac{2159}{T} + 1.075$
(10)	$Fe_2TiO_5 + H_2 = Fe_2TiO_4 + H_2O$	$-2935 - 11.15T$	$\frac{641.4}{T} + 2.437$
(11)	$Fe_2TiO_4 + CO = FeTiO_3 + Fe + CO_2$	$-4603 + 6.52T$	$\frac{1006}{T} - 1.425$
(12)	$Fe_2TiO_4 + H_2 = FeTiO_3 + Fe + H_2O$	$2488 + 0.16T$	$-\frac{543.8}{T} - 0.035$
(13)	$2FeTiO_3 + CO = FeTi_2O_5 + Fe + CO_2$	$314 + 4.08T$	$-\frac{68.6}{T} - 0.89$
(14)	$2FeTiO_3 + H_2 = FeTi_2O_5 + Fe + H_2O$	$7380 - 2.33T$	$-\frac{1613}{T} + 0.509$
(15)	$FeTiO_3 + CO = TiO_2 + Fe + CO_2$	$3340 + 2.2T$	$-\frac{730}{T} - 0.48$
(16)	$FeTiO_3 + H_2 = TiO_2 + Fe + H_2O$	$10400 - 4.26T$	$-\frac{2273}{T} + 0.931$
(17)	$\frac{3}{5}FeTi_2O_5 + CO = \frac{2}{5}Ti_3O_5 + \frac{3}{5}Fe + CO_2$	$10763 + 0.091T$	$-\frac{2352}{T} - 0.02$
(18)	$\frac{3}{5}FeTi_2O_5 + H_2 = \frac{2}{5}Ti_3O_5 + \frac{3}{5}Fe + H_2O$	$17798 - 6.307T$	$-\frac{3890}{T} + 1.378$

Note: $K = P_{CO_2}/P_{CO}$ or P_{H_2O}/P_{H_2}; P_{CO_2}, P_{CO}, P_{H_2O}, and P_{H_2} are the equilibrium partial pressure of CO_2, CO, H_2O, and H_2, respectively; T is the reaction temperature.

the reactions and the equilibrium constants (K) are also listed [22–24]. The reduction of VTM is more complicated than that of ordinary iron ore because the Ti and Fe are symbiotically similar to each.

To investigate the discrepancies in the reduction thermodynamics between VTM and ordinary iron ore with equivalent valence states, the relationship between the $\Delta G^{\ominus}$ and T values in Table 1 can be determined, as shown in Figs. 1(a)–1(d).

As evident from Fig. 1(a), the $\Delta G^{\ominus}$ value of reaction (1) is smaller than that of reaction (9) in the temperature range from 400 to 1600 K. Therefore, Fe_2TiO_5 is more difficult to reduce than Fe_2O_3 in a CO atmosphere at 400–1600 K. According to Fig. 1(b), the $\Delta G^{\ominus}$ value of reaction (7) is also clearly smaller than that of reactions (11), (13), (15), and (17) at 400–1600 K. Thus, Fe_2TiO_4, $FeTiO_3$, and $FeTi_2O_5$ are all more difficult to reduce than FeO in a reducing atmosphere of CO at 400–1600 K. Figs. 1(c) and 1(d) show the same results as Figs. 1(a) and 1(b). Therefore, we concluded that VTM of an equivalent valence state is more difficult to reduce than ordinary iron ore. Interestingly, the $\Delta G^{\ominus}$ values shown in Figs. 1(a) and 1(c) indicate that reducing Fe_2TiO_5 to Fe_2TiO_4 in the oxidized VTM pellets is extremely favorable from a free-energy perspective.

$$\Delta G^{\ominus} = RT \ln \left[\left(\frac{P_{CO_2}}{P_{CO}} \right)_{reality} \Big/ \left(\frac{P_{CO_2}}{P_{CO}} \right)_{balance} \right] \tag{19}$$

$$\Delta G^{\ominus} = RT \ln \left[\left(\frac{P_{H_2O}}{P_{H_2}} \right)_{reality} \Big/ \left(\frac{P_{H_2O}}{P_{H_2}} \right)_{balance} \right] \tag{20}$$

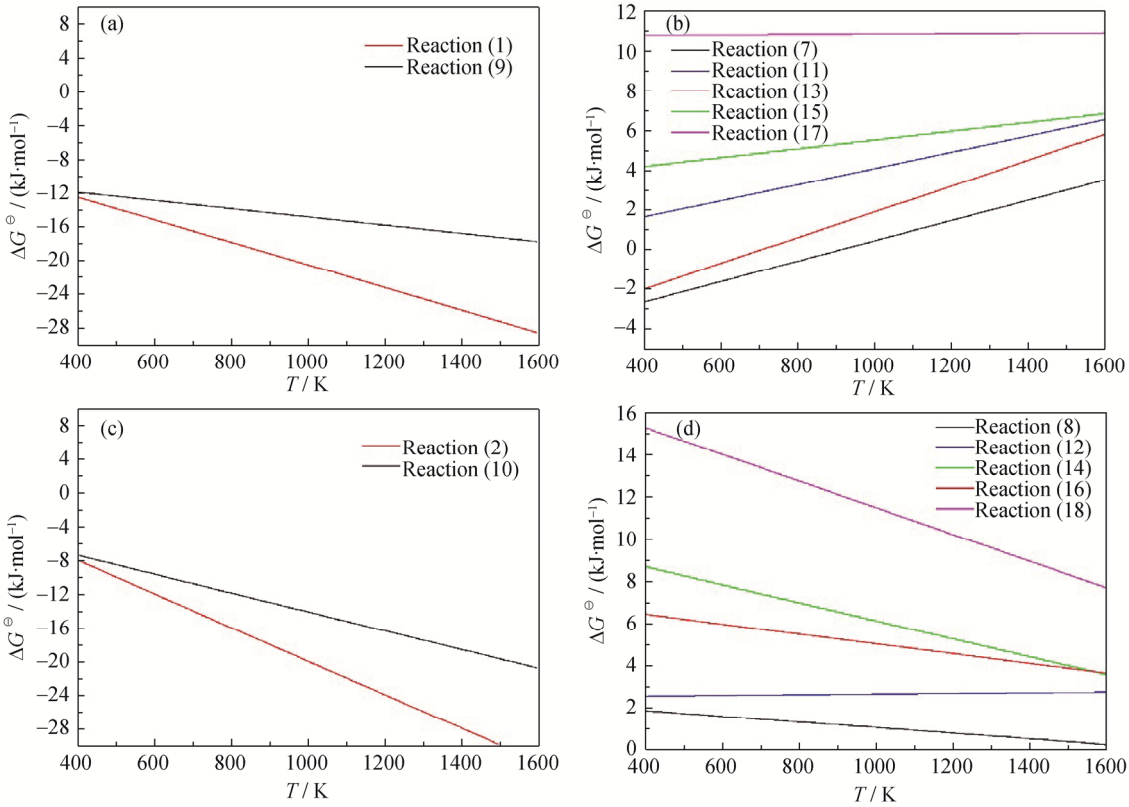

Fig. 1. Relationship between $\Delta G^{\ominus}$ of reduction reactions with the same valence state and T: (a) Fe^{3+} in a CO atmosphere; (b) Fe^{2+} in a CO atmosphere; (c) Fe^{3+} in an H_2 atmosphere; (d) Fe^{2+} in an H_2 atmosphere.

On the basis of the isothermal Eqs. (19) and (20), we conclude that the K values presented in Table 1 determine whether iron and titanium minerals can be reduced at a certain temperature. For instance, when the reduction temperature is 1273 K, the reduction conditions of FeO, Fe_2TiO_4, and $FeTiO_3$ are $K = P_{CO_2}/P_{CO} < 0.480$ or $K = P_{H_2O}/P_{H_2} < 0.764$, $K = P_{CO_2}/P_{CO} < 0.232$ or $K = P_{H_2O}/P_{H_2} < 0.345$, and $K = P_{CO_2}/P_{CO} < 0.0884$ or $K = P_{H_2O}/P_{H_2} < 0.140$, respectively. These conditions are the necessary and basic conditions of the reducing-gas process design used in actual industrial production. In addition, the K values in Table 1 can characterize the stability of oxidized VTM pellets.

In actual production processes, a C–H–O system is used as the main reducing agent. Accordingly, the equilibrium composition of the gas-phase C–H–O–Fe–Ti system is determined by reaction (21). Eq. (22) can be inferred from the $\Delta G^{\ominus}$ of reaction (21):

$$CO + H_2O = CO_2 + H_2, \quad \Delta G^{\ominus} = -7050 + 6.41T \tag{21}$$

$$K = P_{CO_2} \cdot \frac{P_{H_2}}{P_{H_2O} \cdot P_{CO}} = \exp\left(\frac{-\Delta G^{\ominus}}{RT}\right) \tag{22}$$

From Eq. (22), the following relationship can be obtained:

$$\lg \frac{P_{H_2}}{P_{H_2O}} = \lg \frac{P_{CO}}{P_{CO_2}} + \frac{1540}{T} - 1.401 \tag{23}$$

According to the $\lg K = a/T + b$ expression derived from Table 1 and Eq. (23), an equilibrium diagram of oxidized VTM pellets reduced by the C–H–O system can be represented as Fig. 2. This diagram implies that the left side of data points "*BAC*" is a thermodynamically stable zone of Fe_3O_4, whereas the region below "*BAD*" is where FeO is stable. Fig. 2 also indicates that below *EF* is a thermodynamically stable zone for Fe_2TiO_4, that the zone between *EF*, *GH*, and *IJ* is stable for $FeTiO_3$, and that the zone between *GH* and *MN* is stable for $FeTi_2O_5$. Therefore, the reduction of Fe_2TiO_4 proceeds after all free FeO is reduced to Fe. Fig. 3 provides a diagram of the reduction process for the reduction equilibrium for oxidized VTM pellets using the C–H–O system as the reducing agent.

Fig. 2 also reveals that ordinary iron ore and VTM differ from each other in thermodynamics greatly, which affects the characteristics of actual industrial reduction. In addition, it shows that $\left(P_{H_2}/P_{H_2O}\right)_{balance}$ is lower than $\left(P_{CO}/P_{CO_2}\right)_{balance}$ for the reductions of FeO, Fe_2TiO_4, and $FeTiO_3$ when the reduction temperature is greater than 1100 K, which suggests that the reduction capacity of H_2 is higher than that of CO at high temperatures. In actual production processes, H_2 is much better than CO in terms of kinetics. Moreover, some conclusions can be inferred from the trends seen from *GH*, *EF*, and *AD* in Fig. 2. When $FeTiO_3$ is reduced by the H_2–H_2O or CO–CO_2 gas mixtures, the reduction potential of the gas increases with increasing temperature. However, when FeO or Fe_2TiO_4 is reduced, the reduction potential of H_2–H_2O increases with rising temperatures, yet the reduction potential of CO–CO_2 decreases with increasing temperatures. Accordingly, selecting the appropriate reduction temperature and suitable gas composition for different processes is important.

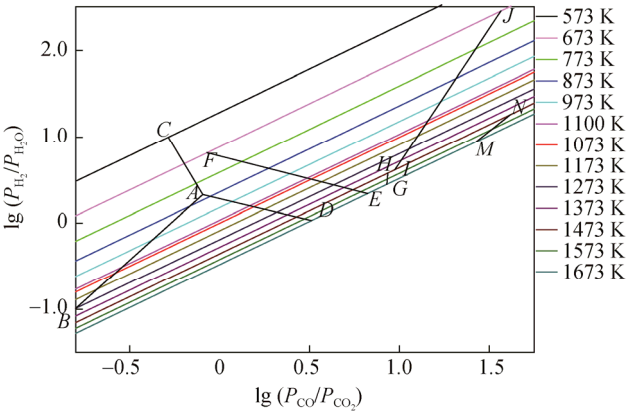

Fig. 2. Reduction equilibrium diagram of oxidized VTM pellets using the C–H–O system as the reducing agent. *AB*—Fe_3O_4 + CO (H_2) = 3FeO + CO_2 (H_2O); *AC*—1/4Fe_3O_4 + CO (H_2) = 3/4Fe + CO_2 (H_2O); *AD*—FeO + CO (H_2) = Fe + CO_2 (H_2O); *EF*—Fe_2TiO_4 + CO (H_2) = $FeTiO_3$ + Fe + CO_2 (H_2O); *GH*—2$FeTiO_3$ + CO (H_2) = $FeTi_2O_5$ + Fe + CO_2 (H_2O); *IJ*—$FeTiO_3$ + CO (H_2) = TiO_2 + Fe + CO_2 (H_2O); *MN*—3/5$FeTi_2O_5$ + CO (H_2) = 2/5Ti_3O_5 + 3/5Fe + CO_2 (H_2O).

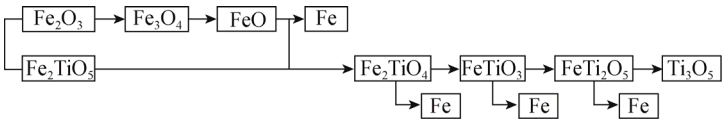

Fig. 3. Reduction process of oxidized pellets of VTM.

3. Experimental

3.1. Preparation of oxidized VTM pellets

VTM samples from the Paixi Area of China were used in this work. The oxidized VTM pellets were prepared by the following steps. First, the VTM was fully mixed with 1wt% binder and 8.5wt% water and then pelletized to a 10–12 mm diameter in a disk pelletizer. Second, the VTM pellets were dried for 4 h in a quartz reactor at 110°C. Finally, the VTM pellets were calcined for 20 min at 1350°C in air. Table 2 lists the main chemical compositions of the oxidized VTM pellets. TFe and TiO_2 were the dominant components in the VTM pellets. X-ray diffraction (XRD) patterns of the oxidized VTM pellets are shown in Fig. 4. The XRD results show that Fe_2O_3 and Fe_2TiO_5 were the main mineral phases of the oxidized VTM pellets.

Table 2. Main chemical compositions of the oxidized VTM pellets wt%

TFe	FeO	TiO_2	SiO_2	Al_2O_3	MgO	CaO	V_2O_5	MnO	S
46.70	0.56	13.20	8.32	6.54	3.28	1.40	0.54	0.42	0.035

3.2. Experimental methods

Approximately 200 g of heated oxidized VTM pellets was directly reacted with reducing gas in a furnace at a reaction pressure of 101325 Pa. The experimental equipment

used in this work is shown in Fig. 5. A tube furnace, a gas mixing chamber, an electronic balance, a high-temperature steel–alloy resistant reactor, and an alundum tube constituted the primary experimental equipment. In the heating course, the reactor was filled with N_2 as protecting gas. After the reaction temperature reached the designated value, the reactor was filled with reactant gas while the mass-change data were continuously recorded by an electronic balance. After the samples were reduced for 240 min, the VTM pellets were cooled to room temperature in a N_2 atmosphere. The cooled VTM pellets were then characterized by XRD.

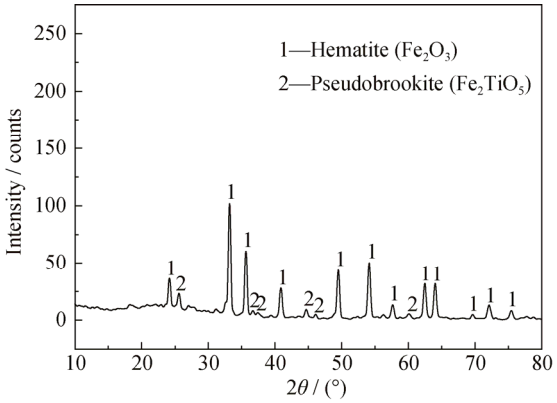

Fig. 4. XRD pattern of the oxidized VTM pellets.

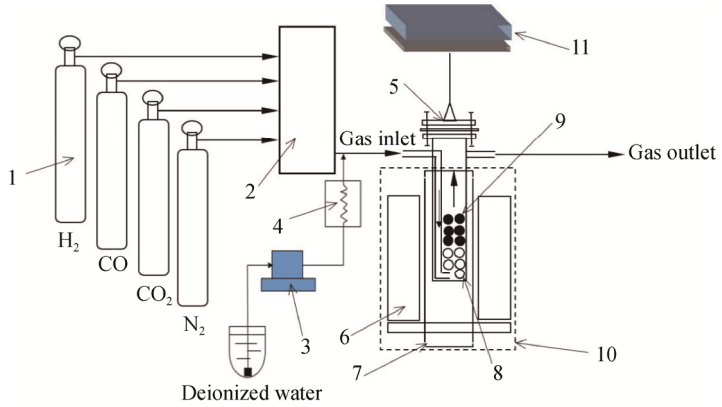

Fig. 5. Schematic of the experimental apparatus. 1—Gas cylinder; 2—Gas mixing chamber; 3—Metering pump; 4—Steam generator; 5—Reactor; 6—Fever zone; 7—Alundum tube; 8—Corundum ball; 9—Oxidized concentrate; 10—Tube furnace; 11—Electronic balance.

The reduction degree of oxidized VTM pellets can be calculated by Eq. (24) [10]:

$$R=\frac{m(\mathrm{O})}{m_0(\mathrm{O})}=\left(\frac{0.11w(\mathrm{FeO})}{0.43w(\mathrm{TFe})}+\frac{m_1-m_2}{m_1\times 0.43w(\mathrm{TFe})}\right)\times 100\% \quad (24)$$

where R is the reduction degree of iron, m_0(O) is the total mass of oxygen bonding with Fe from the oxidized VTM pellets, and m(O) represents the mass loss of oxygen that bonds with Fe during the reduction process. Parameters w(TFe) and w(FeO) are the mass fraction of TFe and FeO in oxidized VTM pellets, m_1 is the mass of the VTM pellet before reduction, and m_2 is the mass of the VTM pellet in the reduction process. The values 0.11 and 0.43 represent the oxygen demand conversion coefficient when converting FeO and Fe to Fe_2O_3, respectively.

4. Results and discussion

4.1. Effect of reduction temperature

The reduction experiments were carried out in the temperature range 673–1373 K at intervals of 100 K and with a gas flow of 5 L/min with 25mol% N_2 and 75mol% H_2 and CO. The molar ratio of H_2 and CO is 1:1. Fig. 6 shows the final reduction degree and the main mineral phases of the reduction products after the pellets were reduced for 240 min at various temperatures. The final reduction degree increased with increasing temperature. The mineral phases of the reduction products also changed at different temperatures. For example, the main mineral phases were Fe_3O_4 and Fe_2TiO_4 at low temperatures. With increasing temperature, the content of FeO increased, whereas that of Fe_3O_4 decreased. FeO and Fe_2TiO_4 could be further reduced to Fe and $FeTiO_3$ with a further increase in temperature. When the temperature reached 1173 K, the $FeTiO_3$ phase disappeared and the main mineral phases of the reduction products were Fe and $FeTi_2O_5$. The $FeTi_2O_5$ content gradually decreased with the continual rise of temperature. On the basis of these experimental results, we concluded that high temperatures promote the reduction of oxidized VTM pellets, consistent with the thermodynamic analysis results. Thus, the recommended reduction temperature for oxidized VTM pellets is approximately 1273–1373 K in actual industrial production.

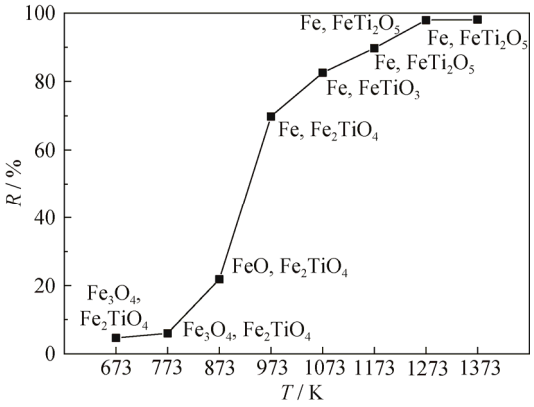

Fig. 6. Final reduction degree and main mineral phases after the pellets were reduced for 240 min at various temperatures.

4.2. Effect of gas composition

To investigate the effect of gas composition on the reduction of oxidized VTM pellets, experiments were carried out at 1273 K for 240 min with a gas flow of 5 L/min with different gas ratios of H_2, CO, H_2O, CO_2, and N_2.

4.2.1. Effect of $H_2/(H_2 + CO)$

To investigate the effect of $H_2/(H_2 + CO)$ on the reduction of oxidized VTM pellets, experiments were performed with $H_2/(H_2 + CO)$ molar ratios of 0, 25mol%, 33.3mol%, 50mol%, 66.7mol%, 75mol%, and 100mol%. The final reduction degree of oxidized VTM pellets and the main mineral phases in the reduction products with different $H_2/(H_2 + CO)$ molar ratios are displayed in Fig. 7. The reduction degree of oxidized VTM pellets increased with increasing $H_2/(H_2 + CO)$ molar ratio. When the molar ratio of $H_2/(H_2 + CO)$ was between 0 and 50mol%, the main mineral phases of the reduction products were Fe and $FeTiO_3$. As the $H_2/(H_2 + CO)$ molar ratio increased, $FeTiO_3$ disappeared, accompanied by the appearance of $FeTi_2O_5$. We concluded that the reduction capacity of H_2 is better than that of CO at high temperatures, which is in accordance with the thermodynamic results. Because H_2 has a smaller molecular diameter than CO, it may experience less gas diffusion resistance during the reduction process, resulting in superior reaction dynamics of H_2 compared with those of CO. Thus, we concluded that hydrogen-rich reduction gas is beneficial to the reduction of oxidized VTM pellets in actual industrial production.

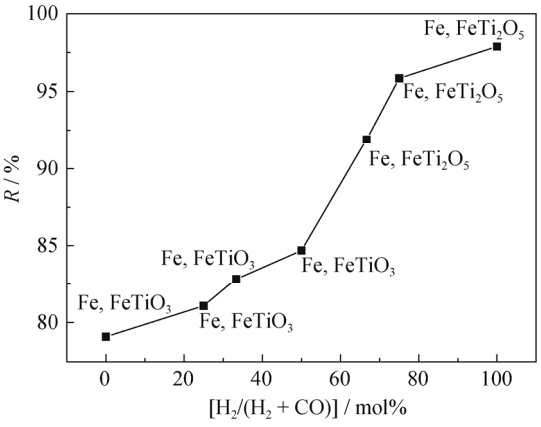

Fig. 7. Final reduction degree and the main mineral phases of the pellets reduced for 240 min in atmospheres of different $H_2/(H_2 + CO)$ molar ratios.

4.2.2. Effect of $CO/(CO + CO_2)$

Experiments were carried out with $CO/(CO + CO_2)$ molar ratios of 10mol%, 30mol%, 50mol%, 70mol%, 80mol%, 90mol%, and 95mol%. Fig. 8 displays the final reduction degree and the main mineral phases of the reduction products after the pellets were reduced for 240 min in atmospheres of different $CO/(CO + CO_2)$ molar ratios. The molar ratio of $CO/(CO+ CO_2)$ strongly affected the reduction of the oxidized VTM pellets, with the reduction degree of VTM pellets increasing with increasing CO content. When the $CO/(CO + CO_2)$ molar ratio was no higher than 70mol%, there was almost no generation of metallic iron in the reduction product. With an increase in the molar ratio of $CO/(CO + CO_2)$, metallic iron is generated. When the molar ratio of $CO/(CO + CO_2)$ was increased to 90mol%, Fe_2TiO_4 disappeared, accompanied by the appearance of $FeTiO_3$. However, with the continuous increase of the $CO/(CO + CO_2)$ molar ratio, Fe and $FeTiO_3$ were still the main mineral phases. These experimental results are generally consistent with the theoretical thermodynamic results. In considering actual industrial production, the molar ratio of $CO/(CO + CO_2)$ should be greater than 90mol% for the efficient reduction of oxidized VTM pellets.

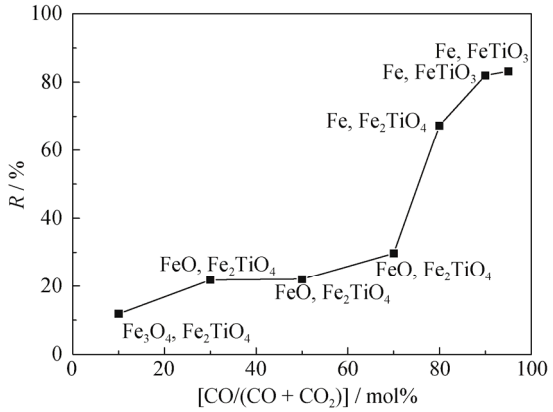

Fig. 8. Final reduction degree and the main mineral phases after the pellets were reduced for 240 min in atmospheres of different $CO/(CO + CO_2)$ molar ratios.

4.2.3. Effect of $H_2/(H_2 + H_2O)$

Experiments were carried out with $H_2/(H_2 + H_2O)$ molar

ratios of 10mol%, 30mol%, 50mol%, 70mol%, 80mol%, 90mol%, and 95mol%. Fig. 9 shows the final reduction degree and the main mineral phases of the reduction products after the VTM pellets were reduced for 240 min in atmospheres with different $H_2/(H_2 + H_2O)$ molar ratios. The results reveal that the reduction degree of VTM pellets increased with increasing $H_2/(H_2 + H_2O)$ molar ratio. When the molar ratio of $H_2/(H_2 + H_2O)$ was no higher than 50mol%, the main mineral phases in the reduction products were FeO and Fe_2TiO_4. As the molar ratio of $H_2/(H_2 + H_2O)$ was increased, metallic iron was generated. When the $H_2/(H_2 + H_2O)$ molar ratio was increased to 80mol%, Fe_2TiO_4 was reduced to $FeTiO_3$. With increasing molar ratio of $H_2/(H_2 + H_2O)$, $FeTiO_3$ disappeared, accompanied by the appearance of $FeTi_2O_5$. A comparison of the results in Fig. 9 with those in Fig. 8 leads to the conclusion that the effect of different $H_2/(H_2 + H_2O)$ molar ratios on the reduction of oxidized VTM pellets is similar to that of different $CO/(CO + CO_2)$ molar ratios, but the effect on the final reduction degree of the former is greater. Moreover, the main mineral phases in the reduction productions were Fe and $FeTi_2O_5$ when the molar ratio of $H_2/(H_2 + H_2O)$ was greater than 90mol%. Therefore, H_2O had less impact on the reduction thermodynamics compared with CO_2 at high temperatures. Thus, the results imply that the molar proportion of $H_2/(H_2 + H_2O)$ is recommended to be more than 90mol% for industrial production.

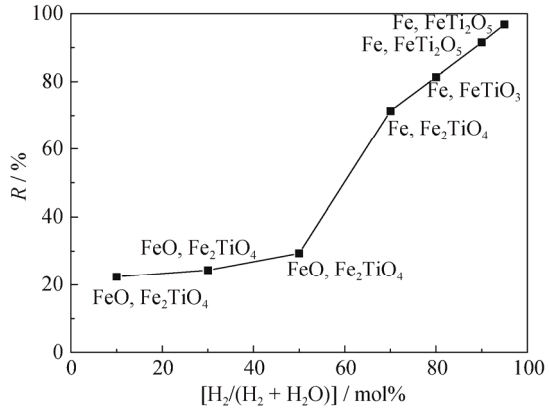

Fig. 9. Final reduction degree and the main mineral phases of the pellets reduced for 240 min in atmospheres with different $H_2/(H_2 + H_2O)$ molar ratios.

4.2.4. Effect of N_2 content

Experiments were performed to investigate the effect of N_2 content on the reduction thermodynamics for the VTM pellets. H_2 and CO (the molar ratio of H_2 and CO is 1:1) were used as reducing agents. The contents of N_2 were 5mol%, 25mol%, 50mol%, 75mol%, 90mol%, and 95mol%. The final reduction degree of oxidized VTM pellets and the main mineral phases of the reduction products with different contents of N_2 are shown in Fig. 10. When the content of N_2 was greater than 95mol%, only trace amounts of metallic iron were produced. As the content of N_2 was lowered, metallic iron appeared gradually. When the content of N_2 reached 75mol%, the FeO phase disappeared completely and the main mineral phases were Fe and Fe_2TiO_4. With a further decrease of N_2, Fe_2TiO_4 was reduced to $FeTiO_3$. When the content of N_2 ranged from 25mol% to 50mol%, the final reduction degree and the main mineral phases remained constant. As the content of N_2 was further decreased, the $FeTiO_3$ phase disappeared, with an increased content of $FeTi_2O_5$ and an elevated reduction degree. From these results, the content of N_2 had little impact on the reduction of oxidized VTM pellets. Nevertheless, on the basis of the results of these experiments, to ensure that the oxidized VTM pellets have a higher reduction degree, the content of N_2 should not be greater than 25mol% in actual production.

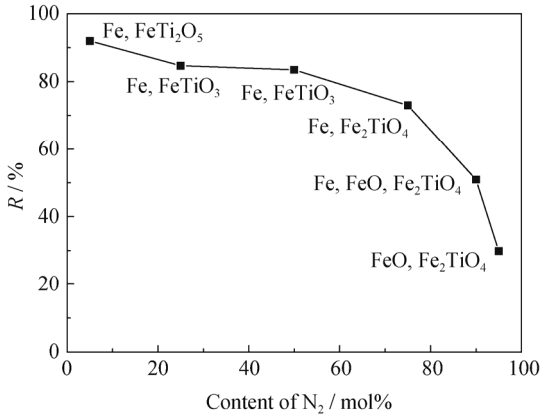

Fig. 10. Final reduction degree and the main mineral phases of the pellets reduced for 240 min with different contents of N_2.

4.3. Effect of iron ore

Oxidized Australian ore (AO) pellets with particle sizes of 10–12 mm were prepared using the same method as that used to prepare the oxidized VTM pellets. The reduction results of oxidized AO pellets and oxidized VTM pellets in the temperature range 973–1373 K are compared in Fig. 11. Other specific experimental conditions were also controlled: the total gas flow was 5 L/min with 25mol% N_2 and 75mol% H_2 and CO, and the molar ratio of H_2 and CO is 1:1. The reduction experiments were carried out in the temperature range 673–1373 K at intervals of 100 K and with a gas flow of 5 L/min. The final reduction degree of oxidized VTM pellets was clearly much lower than that of oxidized AO pellets when the temperature was less than 1273 K. A comparison of the main mineral phases of the two reduction products reveals that the reduction of Ti-containing iron minerals (such as Fe_2TiO_4, $FeTiO_3$, and $FeTi_2O_5$) requires greater thermody-

namic conditions than the reduction of FeO, which is consistent with the theoretical thermodynamic analysis results. Therefore, we concluded that the reduction degree can be limited by Ti-containing iron minerals in oxidized VTM pellets.

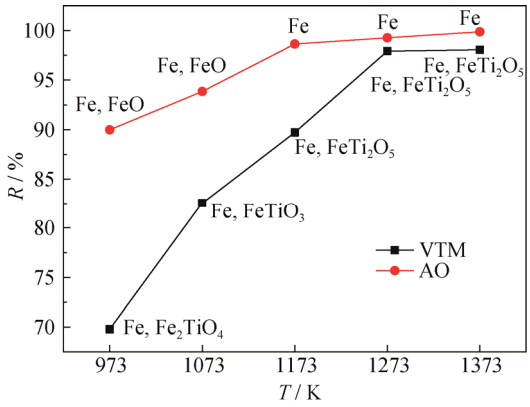

Fig. 11. Comparison of the final reduction degree and the main mineral phases between oxidized VTM pellets and oxidized AO pellets reduced for 240 min.

5. Conclusion

Thermodynamic studies on the reduction of oxidized VTM pellets were systematically carried out in an atmosphere of the C–H–O system as a reducing agent. A reduction equilibrium diagram of oxidized VTM pellets using the C–H–O system as a reducing agent was obtained. The results indicate that the reduction of Fe_2TiO_5 to Fe_2TiO_4 is easy to achieve from a free-energy perspective, whereas Fe_2TiO_4 cannot be reduced until the free FeO is completely reduced to Fe. Additionally, the reduction process of oxidized VTM pellets was clearly described, revealing that the thermodynamic behavior of ordinary iron ore is much different from that of VTM. We determined that Ti-containing iron minerals in oxidized VTM pellets can restrict the reduction degree of production. Experiments were performed to investigate the effects of the reduction temperature, gas composition, and two types of iron ore on the reduction of oxidized VTM pellets. We concluded that the final reduction degree increases with increasing reduction temperature, increasing $H_2/(H_2 + CO)$ molar ratio, and decreasing levels of H_2O, CO_2, and N_2. In addition, according to the main mineral phases of the reduction products, the reduction processes of the oxidized VTM pellets were analyzed under different conditions. All of the results of the reduction experiments were consistent with those of thermodynamic analysis.

Combining the theoretical thermodynamic analysis results and the experimental results, we deduced several suggestions to obtain a higher reduction degree of oxidized VTM pellets in actual industrial production: the reduction temperature should be approximately 1273–1373 K, a hydrogen-rich reducing agent should be used if possible, the content of H_2O or CO_2 in the reducing agent should be less than 10mol%, and the content of N_2 in the reducing agent should not be greater than 50mol%.

Acknowledgement

This work was financially supported by the Ministry of Land and Resources Public Welfare Industry Research Project, China (No. 201511062-02).

References

[1] A.M. Alfantazi and R.R. Moskalyk, Processing of indium: a review, *Miner. Eng.*, 16(2003), No. 8, p.687.

[2] S.Y. Chen and M.S. Chu, Metalizing reduction and magnetic separation of vanadium titano-magnetite based on hot briquetting, *Int. J. Miner. Metall. Mater.*, 21(2014), No. 3, p. 225.

[3] T. Hu, X.W. Lv, C.G. Bai, Z.G. Lun, and G.B. Qiu, Reduction behavior of panzhihua titanomagnetite concentrates with coal, *Metall. Mater. Trans. B*, 44(2013), No. 2, p. 252.

[4] L.H. Zhou and F.H. Zeng, Reduction mechanisms of vanadium–titanomagnetite–non-coking coal mixed pellet, *Ironmaking Steelmaking*, 38(2014), No. 1, p. 59.

[5] R.J. Longbottom, O. Ostrovski, J.Q. Zhang, and D. Young, Stability of cementite formed from hematite and titanomagnetite ore, *Metall. Mater. Trans. B*, 38(2007), No. 2, p. 175.

[6] Y.L. Sui, Y.F. Guo, T. Jiang, X.L. Xie, S. Wang, and F.Q. Zheng, Gas-based reduction of vanadium titano-magnetite concentrate: Behavior and mechanisms, *Int. J. Miner. Metall. Mater.*, 24(2017), No. 1, p. 10.

[7] J. Dang, X.J. Hu, G.H. Zhang, X.M. Hou, X.B. Yang, and K. Chou, Kinetics of reduction of titano-magnetite powder by H_2, *High Temp. Mater. Processes*, 32(2013), No. 3, p. 229.

[8] J. Tang, M. Chu, C. Feng, Y. Tang, and Z. Liu, Coupled effect of valuable components in high-chromium vanadium-bearing titanomagnetite during oxidization roasting, *ISIJ Int.*, 56(2016), No. 8, p. 1342.

[9] S.Y. Chen and M.S. Chu, Metalizing reduction and magnetic separation of vanadium titano-magnetite based on hot briquetting, *Int. J. Miner. Metall. Mater.*, 21(2014), No. 3, p. 225.

[10] Y.L. Sui, Y.F. Guo, T. Jiang, and G.Z. Qiu, Reduction kinetics of oxidized vanadium titano-magnetite pellets using carbon monoxide and hydrogen, *J. Alloys Compd.*, 706(2017), p. 546.

[11] H.Y. Sun, A.A. Adetoro, F. Pan, Z. Wang, and Q.S. Zhu, Effects of high-temperature preoxidation on the titanomagnetite ore structure and reduction behaviors in fluidized bed, *Metall. Mater. Trans. B*, 48(2017), No. 3, p. 1898.

[12] O.N. Salmon, R.E. Fayling, G.E. Gurr, and V.W. Halling, Thermodynamics of post-erasure signal effect in γ-Fe_2O_3 magnetic recording tapes, *IEEE Trans. Magn.*, 15(1979), No. 5, p. 1315.

[13] M.E. Gálvez, P.G. Loutzenhiser, I. Hischier, and A. Steinfeld, CO_2 splitting via two-step solar thermochemical cycles with Zn/ZnO and FeO/Fe_3O_4 redox reactions: Thermodynamic analysis, *Energy Fuels*, 22(2008), No. 5, p.3544.

[14] T. Katsura, M. Wakihara, S.I. Hara, and T. Sugihara, Some thermodynamic properties in spinel solid solutions with the Fe_3O_4 component, *J. Solid State Chem.*, 13(1975), No. 1-2, p. 107.

[15] H. Sun, X. Dong, X. She, Q. Xue, and J. Wang, Solid state reduction of titanomagnetite concentrate by graphite, *ISIJ Int.*, 53(2013), No. 4, p. 564.

[16] E. Park and O. Ostrovski, Reduction of titania–ferrous ore by carbon monoxide, *ISIJ Int.*, 43(2003), No. 9, p. 1316.

[17] W. Yu, Q.Y. Tang, J.A. Chen, and T.C. Sun, Thermodynamic analysis of the carbothermic reduction of a high-phosphorus oolitic iron ore by FactSage, *Int. J. Miner. Metall. Mater.*, 23(2016), No. 10, p. 1126.

[18] R.B. Wanty and M.B. Goldhaber, Thermodynamics and kinetics of reactions involving vanadium in natural systems: Accumulation of vanadium in sedimentary rocks, *Geochim. Cosmochim. Acta*, 56(1992), No. 4, p. 1471.

[19] Y.J. Gu, J.B. Cao, J.Q. Wu, and L.Q. Chen, Thermodynamics of strained vanadium dioxide single crystals, *J. Appl. Phys.*, 108(2010), No. 8, art. No. 083517.

[20] G.H. Emmons and W.S. Williams, Thermodynamics of order-disorder transformations in vanadium carbide, *J. Mater. Sci.*, 18(1983), No. 9, p. 2589.

[21] O. Delaire, M. Kresch, J.A. Muñoz, M.S. Lucas, J.Y.Y. Lin, and B. Fultz, Electron-phonon interactions and high-temperature thermodynamics of vanadium and its alloys, *Phys. Rev. B*, 77(2008), art. No. 214112.

[22] R.H. Sievwright, J.J. Wilkinson, H.S.C. O'Neill, and A.J. Berry, Thermodynamic controls on element partitioning between titanomagnetite and andesitic–dacitic silicate melts, *Contrib. Mineral. Petrol.*, 172(2017), p. 62.

[23] R.O. Sack and M.S. Ghiorso, An internally consistent model for the thermodynamic properties of Fe–Mg-titanomagnetite-aluminate spinels, *Contrib. Mineral. Petrol.*, 106(1991), No. 4, p. 474.

[24] R. Aragón and R.H. Mccallister, Phase and point defect equilibria in the titanomagnetite solid solution, *Phys. Chem. Miner.*, 8(1982), No. 3, p. 112.